



Published in final edited form as:

Polymer (Guildf). 2015 May 1; 64: 100–111. doi:10.1016/j.polymer.2015.03.021.

MALDI-TOF/TOF CID Study of Poly(1,4-dihydroxybenzene terephthalate) Fragmentation Reactions

Anthony P. Gies[#], Sarah M. Stow, John A. McLean, and David M. Hercules^{*}

Department of Chemistry, Vanderbilt University, Nashville, TN 37235

Abstract

MALDI-TOF/TOF collision-induced dissociation (CID) experiments were conducted on model aromatic polyester oligomers. CID fragmentation studies identified initial fracture of the ester bond and subsequent CO loss as a major pathway, consistent with the general fragmentation mechanism used to explain the origin of poly(*p*-phenylenediamine terephthalamide) (PPD-T) fragment ions. Specifically, both charge-remote and charge-site fragmentation were observed. Different parent-ion species were observed, the major ones being carboxyl-hydroxyl, di-carboxyl, di-hydroxyl, and phenyl-carboxyl terminated. One species observed was hydroxyl-diethylamine terminated caused by reaction of carboxyl groups with triethylamine added to the synthesis reaction mixture. Fragment ions reflected the end groups of the parent oligomers. Some MALDI fragment-ion spectra were obtained for species showing exchange between Li and H at the carboxyl end group. Bond energy calculations provide further insight into suggested fragmentation mechanisms.

1. Introduction

In a recent study of poly(*p*-phenylenediamine terephthalamide) (PPD-T) polymers we used the evaporation-grinding (E-G) sample preparation method for MALDI studies of CID fragmentation reactions [1]. The present work combines the E-G MALDI sample preparation method with TOF/TOF CID fragmentation to examine the chemical structures of model poly(1,4-dihydroxybenzene terephthalate) (DHB-T) oligomers. The overall goal was to determine the CID fragmentation mechanism of aryl polyesters, particularly because they lack aliphatic hydrogens. Based on CID identification of an aryl polyester main-chain weak link at the ester C(O)-O bond, comparable to a similar weak link for aramids at the C(O)-NH bond, we were able to further expand the utility of our general aramid fragmentation mechanism. This study helps to identify the origin of side products, such as triethylamine-based side reactions leading to end group modification. Bond energy calculations provide further insight into suggested fragmentation mechanisms.

^{*}Corresponding Author: Prof. David M. Hercules, Department of Chemistry, Vanderbilt University, Nashville, TN 37135 USA. Telephone: (615)343-5230. david.m.hercules@vanderbilt.edu.

[#]Present address: Department of Core R&D Analytical Sciences, The Dow Chemical Company, 2301 N. Brazosport Blvd., B-1219, Freeport, TX 77541

Publisher's Disclaimer: This is a PDF file of an unedited manuscript that has been accepted for publication. As a service to our customers we are providing this early version of the manuscript. The manuscript will undergo copyediting, typesetting, and review of the resulting proof before it is published in its final citable form. Please note that during the production process errors may be discovered which could affect the content, and all legal disclaimers that apply to the journal pertain.

A number of MALDI TOF/TOF CID studies of aliphatic polyesters have been reported; they are summarized in two recent reviews [2,3]. Two detailed studies of poly(butylene adipate) have appeared [4,5]. Most MALDI studies of polyesters have dealt with entirely aliphatic materials. Recently, the Pasch group has reported MALDI [6] and electrospray [7] studies of partially aromatic polyesters, but not CID. To the best of our knowledge no MALDI (or electrospray) studies of wholly aromatic polyesters exist, probably because of their insolubility. Using the evaporation-grinding sample preparation method [8] has allowed us to obtain MALDI spectra of entirely aromatic polyesters and to investigate their collision-induced decomposition.

2. Experimental

2.1 Polymerization of Poly(1,4-dihydroxybenzene terephthalate)

Poly(1,4-dihydroxybenzene terephthalate) (DHB-T) was synthesized via solution polymerization [9]. All reagents were obtained from commercial sources and used as received. To a well-dried, 250-mL three necked flask, with nitrogen inlet/outlets and magnetic stirrers, 140.0 mL of dry dichloromethane (Fisher) and 3.00 g (27.3 mmol) of 1,4-benzenediol were added. To this mixture, 26.5 mL of triethylamine (Aldrich), and 18.9 g of triethylamine hydrochloride (Aldrich) were added with stirring. Subsequently, with rigorous stirring, 6.00 g (29.5 mmol) of terephthaloyl chloride (Aldrich) were added to achieve a diol-to-diacid chloride molar ratio of 48:52. Stirring was continued for 60 min. until the temperature reached 28 °C. Then the reaction was terminated with a large volume of distilled water, yielding a fibrous precipitate. The precipitate was filtered and washed thoroughly by distilled water containing ~1% acetic acid. The experimental conditions (i.e., relatively short reaction times) were chosen to insure that the reactions would yield low molecular weight aryl polyester powders. The structures of the oligomers formed were assumed to be those shown in Table 1.

2.2 MALDI-TOF/TOF CID Measurements

All samples were analyzed using an Applied Biosystems 4700 Proteomics Analyzer MALDI-TOF/TOF instrument (Applied Biosystems, Framingham, MA) equipped with a 355 nm Nd:YAG laser. All spectra were obtained in the positive ion mode using an accelerating voltage of 8 kV for the first source and 15 kV for the second source and a laser intensity of ~10% greater than threshold. Instrument voltages were optimized for each spectrum to achieve the best signal-to-noise ratio. External mass calibration was performed using protein standards from a Sequazyme Peptide Mass Standard Kit (Applied Biosystems) and a three-point calibration method using Angiotensin I ($m = 1296.69$ Da), ACTH (clip 1–17) ($m = 2093.09$ Da), and ACTH (clip 18–39) ($m = 2465.20$ Da). Internal mass calibration was subsequently performed using a PEG standard ($M_n = 2000$; Polymer Source, Inc.) to yield monoisotopic mass accuracy better than $m = \pm 0.05$ Da. The instrument was calibrated before each measurement to ensure constant experimental conditions.

The CID collision energy is defined by the potential difference between the source acceleration voltage and the floating collision cell; in our experiments this voltage difference was set to 1 kV. Air was used as a collision gas at pressures of 1.5×10^{-6} and 5×10^{-6} Torr

(which will be referred to as “low” and “high” pressure, respectively). All spectra were acquired in the reflection mode with a mass resolution greater than 3000 full-width at half-maximum height (fwhm); isotopic resolution was observed throughout the entire mass range detected. MALDI spectra were run in a dithranol (Aldrich) matrix doped with sodium trifluoroacetate (NaTFA; Aldrich). Polymer samples were prepared using the evaporation-grinding method (E-G method) [8] in which a 2 mg sample of polymer was ground to a fine powder with 60 μL of distilled tetrahydrofuran (THF, Fisher) in an agate mortar and pestle. The molar ratios of matrix:NaTFA:polymer were 25:1:1. The mixture was then ground a second time to ensure homogeneity. A sample of the mixture was then pressed into a sample well, by spatula, on the MALDI sample plate. MS and MS/MS data were processed using the Data Explorer 4.9 software (Applied Biosystems).

2.3 Bond Energy Calculations

The bond energies for DHB-T and its amide were determined by two different approaches using Gaussian09 software [10]. First, the parent structure was optimized followed by independent optimizations of the two fragment structures. In this approach the energies of the two independent structures were added together and then subtracted from the energy of the parent structure to give the energy of the broken bond. The independent fragments were determined to have doublet multiplicity due to the single-electron radical on each fragment resulting from homolytic bond cleavage. The second approach consisted of optimizing the parent structures and then optimizing the two fragments resulting from the homolytic bond cleavage present together in the calculation. The two structures were placed $\sim 15 \text{ \AA}$ apart to ensure that they would not interact with each other. The two fragments together were determined to have triplet multiplicity due to each of the two fragments having one unpaired electron from the homolytic bond cleavage. The total energy of the optimized two fragments was then subtracted from the energy of the parent structure to give the energy of the broken bond. The energies (kcal/mol) for both the doublet and triplet treatments of the homolytic bond cleavage agreed almost exactly with one another as can be seen in Figure 1, giving credence to their numerical validity. Note that the C(O)-N bond is the second weakest bond in the amide and that the Ph-C(O) bond is also weakened. DFT/B3LYP/6-31G* level of theory was used for all the calculations and they were performed *in vacuo* and in the ground state.

3. Results and Discussion

We will first define the nomenclature to be used in this study and then present the TOF/TOF CID fragmentation of a model aryl polyester oligomer. Based on the findings for the model aryl polyester oligomer, we will present some general aryl polyester fragmentation mechanisms to explain the fragment species identified in the TOF/TOF CID mass spectra. The discussion will also focus on the similarities and differences between the CID fragmentation of aryl polyesters and other polymers.

3.1 Nomenclature

Terminology – All figures will show structures and peaks labeled according to the following key:

- i. precursor ion peaks are labeled in the x-y format (x = table number, y = structure number for precursor ions with letters denoting end groups where appropriate). The table number and structure indication may be followed by the ion that provides the charge added to the oligomers during the MALDI process (e.g. Na⁺, Li⁺ or M⁺ for generic metal) where such indication is important;
- ii. precursor ion backbone and end-group modification labels are kept consistent with our previous publications [11], except in the present case where N = a diethylamine end-group and Q = a carboxyl end group that has reacted with a 3-aminoquinoline MALDI matrix molecule; cyclic oligomers are so indicated;
- iii. fragment ions will be identified by their two end groups according to the following:

B – Carbonyl	N – Diethylamine or Ethylamine
OH – Hydroxyl	Q – 3-Aminoquinoline adduct
C – Carboxyl	O – Ring Carbonyl
D – C ₆ H ₄	P – C ₆ H ₅

- iv. when indicated, the number of repeat units (*n*) corresponding to the mass numbers appropriate to the structure.

For example, a precursor ion peak labeled “1-1NLi⁺” corresponds to structure 1-1N in Table 1 which has a diethylamine end-group modification (N), lithium cationization (Li⁺), and an undefined number of aryl polyester repeat units. Similarly, a CID *fragment* peak labeled “ND₁Li⁺” corresponds to a radical fragment that is end-group modified by attachment of a diethylamine group (N) on one chain end and decarboxylation (D) on the other chain end, lithium cationization (Li⁺), and has a single aryl polyester repeat unit (*n* = 1). The mass ranges are listed in the tables for ions in the mid-mass range having different “*n*” values. Mass peaks will be described in the order of decreasing abundance and categorized as major, medium, or small, based on their relative intensities. As a companion to the figures, we present two tables indicating structures of unfragmented MALDI precursor ions and fragment ions produced by low effective kinetic energy TOF/TOF CID fragmentation.

3.2 MALDI Spectra of DHB-T

Figure 2 shows the MALDI-TOF mass spectra of poly(1,4-dihydroxybenzene terephthalate) (DHB-T) for sodium (2A) and lithium (2B) cationization. The insets in the spectra show that the DHB-T species seen are mostly independent of the cation used and have approximately the same relative intensities. Cation exchanged species are an exception, they are more intense for Li. For example, compare the relative intensities of the 761.2 Da and 783.2 Da peaks in Fig. 2A with those at 745.2 and 751.2 Da in Fig. 2B. Similarly, there is only a single peak at 909.2 Da in Fig. 2A but there are three peaks in the vicinity of 900 Da in Fig. 2B. A total of fourteen species were observed in the DHB-T MALDI spectra, and their proposed structures are given in Table 1 along with their masses in the middle-mass range. The masses enclosed in < > are listed for metal ion exchanged species. Not all species were observed in all spectra for different sample preparations. The species observed are consistent

with the monomer ratios used for synthesis, the diacid chloride was added in slight excess to counter side reactions. Closer inspection of Figure 2 identifies the presence of some end group side reactions: (1) species 1-1, 1-3, 1-5 and 1-6 undergo significant H-metal ion exchange at the carboxyl end group; (2) transamination reactions occur at the carboxyl end groups during synthesis, *vide infra*, to produce species 1-1N and 1-3N; and (3) a side reaction occurs between end groups and the 3-aminoquinoline MALDI matrix to produce species 1-1Q and 1-3Q.

Table 2 summarizes the percent total ion currents (%TIC) measured for the species listed in Table 1 for both Na and Li cationization. The three columns on the left in Table 2 (2L) give the %TIC data for each of the individual species observed in the MALDI spectra of DHB-T. The three columns on the right (2R) give the aggregated data for each of the DHB-T oligomers (*vide infra*). Three separate spectra were analyzed to obtain the data listed in Table 2 for both Na and Li cationization; spectra were chosen on the basis of signal-to-noise ratio.

The sum of the intensities of all members of a given species (e.g., 1-1 with different n values) in each spectrum was measured; the intensities of all species so calculated were summed for each spectrum and this was taken as the total ion current (TIC) for that spectrum. The percentages of the ion currents (%TIC) were calculated for each species in each spectrum and the results for the three spectra were averaged. The average values are shown in Table 2. In Table 2L, the hydroxyl-carboxyl (Species 1-1) and hydroxyl-hydroxyl (Species 1-2) terminated oligomers are the major individual species produced in both the Na- and Li-cationized MALDI spectra. Species 1-3 and 1-3Q are the third and fourth most intense for Na cationization; 1-1M is third and 1-1Q and 1-8 are fourth for Li cationization. Note that species 1-8 is not seen in the Na-cationized MALDI spectra. Comparing the insets of Figures 2A and 2B, it would appear that sodium should be the preferred cation for studying CID of aryl polyesters. However, lithiated precursor ions gave better signal-to-noise ratios in the CID fragmentation spectra. Therefore, all CID spectra described will be for lithium cationized oligomers.

Closer inspection of Table 2L reveals that many of the individual species observed are derivatives of DHB-T oligomers. For example, 1-1N must be formed by reaction of 1-1 with triethylamine during synthesis. On the other hand, 1-3Q must be formed by reaction of the 1-3 oligomer with the 3-aminoquinoline matrix – a MALDI artifact. Therefore, to obtain a better idea about the relative amounts of the different oligomers formed in synthesis, the aggregate intensities for each oligomer are presented in Table 2R. For example, the value for Na cationization of oligomer 1-1 in Table 2R is the sum of intensities for species 1-1, 1-1M, 1-1N, 1-1Q and 1-1NM. Similarly, the value for Li cationization of oligomer 1-3 is the sum of intensities for 1-3, 1-3Q, 1-3M, 1-3MM and 1-3N. Here also the values are averages of distributions calculated for three separate spectra. Oligomers 1-1, 1-2, and 1-3 have the greatest summed intensities, as would be expected from synthesis.

Table 2 also indicates that not all species are observed in both Na- and Li-cationized MALDI spectra; some species having low %TIC values are seen for Na cationization, but not for Li. In all probability this is an effect of the better signal-to-noise ratios for the Na

cationized MALDI spectra. The most interesting case is species 1-8, not seen for Na cationization, but being 14.2 %TIC for Li. Because the 1-8M Li-exchanged species is also observed, structure 1-8 probably has a terminal carboxyl group. The structure given in Table 1 is consistent with the mass observed, but it is difficult to see how it could be formed either by chemical reaction in the synthesis or as a MALDI artifact.

Estimating the relative amounts of oligomers formed in synthesis from the data of Table 2R is risky, because the response factors for the specific oligomers are not known. However, it is clear that some species seen in Table 1 are formed at the expense of 1-1 and 1-3. Adding together the %TIC values for the combinations in Table 2R indicates that the amounts of species 1-1 and 1-3 are underestimated in Table 2L, especially species 1-3. However, because of similar structures, it is probable that the response factors for the different species are similar, so one can say that, at least qualitatively, species 1-1, 1-2, and 1-3 are the major products of synthesis, 1-5 and 1-6 are medium, with the others being minor, except for the problem of 1-8 in the Li-cationized spectra.

Recently the Pasch group published a paper on the MALDI spectra of polymers formed from phthalic acid (PA) and propylene glycol (PG) [6]. Oligomeric species were obtained having some of the end group combinations reported for DHB-T in Table 1. The two major species were PG-[PA+PG]_n-H and HO-[PA-PG]_n-H (abbreviations from their paper) corresponding to species 1-2 and 1-1, respectively, from Table 1. A major difference was that their analog to species 1-3 was seen only weakly; it has the second highest aggregate %TIC in Table 2R. This is consistent with the difference in synthesis conditions – they used a 30% excess of diol and we used a diol:acid ratio of 48:52. Another difference was that they saw a greater intensity of cyclic species than is shown in Table 2. This probably reflects the difference in flexibility of the diol units. 1,4-Dihydroxybenzene is much less flexible than propylene glycol, limiting the ability to form cyclic polymers. Oligomers comparable to the phenyl-ring terminated species, such as 1-4, 1-5, 1-6 and 1-7, were not observed even though they account for about 25% TIC for Na-cationized species in Table 2.

3.3 MALDI-TOF/TOF CID Fragmentation

3.3.1 DHB-T Precursor Structure 1-1—Figure 3A shows the MALDI-TOF/TOF CID spectrum for the lithium cationized hydroxyl-carboxyl capped structure of DHB-T (Structure 1-1, 985.2 Da, $n = 4$). The hydroxyl-carboxyl terminated oligomer will be used as the model for our discussion of MS/MS for species observed in the MALDI spectra of aryl polyesters. Initial inspection of the major fragment-ion peaks in the CID spectrum (Fig. 3A), reveal the following series: (1) species DOH_n (220.1, 460.1, 700.2 and 940.2 Da); (2) CD(1)_n. (128.0, 368.1, 608.1 and 848.2Da); (3) BOH_n* (241.1 and 481.1 Da); (4) CB_n* (149.0, and 389.1Da); and (5) OO (p-benzoquinone) that arises from double cleavage of the COO bonds on a phenyl group and is not a member of a prominent series (115.0 Da). Structures of the fragment ion species are given in Table 3.

Table 4 lists the fragment ions and their %TIC for for the six oligomeric species of DHB-T for which it was possible to obtain reproducible MS/MS spectra. Percent TIC was calculated by adding the currents of the species that, in sum, constitute >99% of the observed fragment-ion current intensities in a given oligomer's MS/MS spectra and (where possible) are seen

consistently in the spectra of oligomers $n = 2-4$. The procedure is described in detail in an earlier paper [1]. Table 4 is structured in the following way. The first five rows (A1-B3) are for the fragment ions generated for each oligomer according to the mechanism given in Scheme 1. The next row (Subtotal) gives the subtotal of %TIC for these five species for each oligomer. The next four rows list small fragment ions that are commonly observed in the MS/MS spectra of the six species listed. The lowest two rows are for fragment ions that are unique to a specific oligomer/species.

Three factors are important for determining polymer degradation mechanisms: (1) bond dissociation energies (the weakest bonds generally break first), (2) stability of the radicals generated by fragmentation [12], and (3) reactions that do not involve direct main chain fracture, such as hydrogen-atom transfer. For DBH-T, the bond dissociation energies from Figure 1 predict that the order of DBH-T bond breaking (weakest to strongest) would be: O-C(O) > Ph-C(O)/ Ph-O > Ph-COOH, obviously different from what is observed. The apparent fracture is that of a phenyl-carbonyl bond. This difference arises because ions having CO-terminated phenyl groups produced by carbonyl-O fracture are unstable relative to CO loss and generation of stable phenyl radicals (*vide infra*). It is noteworthy that hydrogen-transfer reactions (both 1,5-H and cross chain-H transfer) typically trump main-chain fracture in the CID of aliphatic polyesters [5,13], and polyurethanes [11]. H-transfer reactions are not significant in aromatic polyesters because the oligomers lack readily extractable hydrogens and the diols are more rigid.

Two different types of fragmentation reactions are important for the aromatic polyesters: charge-remote and charge-site fragmentation. It is assumed that the Li is bound to the carboxyl group(s) to form a complex. In charge-remote fragmentation of aromatic polyesters initial chain fracture occurs at a C(O)-O site remote from the Li cation; the charge on the fragment is provided by retention of the Li cation. In charge-site fragmentation chain fracture occurs at the cationized site and the Li ion remains bonded to one of the two organic fragments but its formal charge can be transferred to the other fragment, generating a charged species that does not contain Li. In the case of DHB-T the Li could end up bonded to either a phenolic oxygen or a carboxyl group.

Scheme 1 shows the major fragmentation mechanisms for the hydroxyl-carboxyl oligomer (1-1) of DHB-T for $n=4$ (985.2 Da, Fig. 3A). The charge-remote reactions are shown at the top (Scheme 1-A). The two C(O)-O groups can fragment yielding different end groups on the initially produced ion. In both reactions A-1 and A-2 a phenyl-C=O radical is produced initially that loses CO to give species CD(1) in A-1 and DOH in A-2. Charge is retained on each fragment remote from the reaction site. The 356 and 304 Da radicals are unstable, typical of phenoxy radicals. It should be noted that species DOH and CD(1) together account for nearly 50% TIC for oligomer 1-1 as seen in Table 4.

The pathway for charge-site fragmentation is shown in Scheme 1-B. In Reactions B-1 and B-2, the Li at the reaction site becomes covalently bonded to a phenoxy oxygen, splitting the carboxyl group and generating the charged species, CB* with one end group (-COOH) and species BOH* with the other (-OH). Note that the reaction has essentially transferred the formal charge from the Li to the organic moiety. Reaction B-3 shows that it is possible to

generate a third species, CD(2)*, an isobar of BOH, by the Li bonding to a carboxyl group for the uncharged fragment. Species CB* and BOH* together account for about 15% of the total ion current (Table 4). Inspection of Table 4 shows that the fragment ions generated by the reactions in Scheme 1 account for about 70% TIC for the 1-1 oligomer. This is typical of all six species shown in Table 4 with an average value of 65% TIC. Li cationized MS/MS spectra typically show intense low mass fragment ions, the four most common ones are given in Table 4: DB*, BB(1), OO, and OOH(1). Ion DB* is the most intense of these for all six species studied. Oligomer 1-1 does not show any unusual fragment ion, different from the others.

3.3.2 DHB-T Precursor Structure 1-1Li—Figure 3B shows the MALDI-TOF/TOF CID spectrum for the lithium cationized, lithium exchanged hydroxyl-carboxyl terminated oligomer of DBH-T (Structure 1-1Li, 751.2 Da, $n=3$). Exchange has occurred between Li and H at the carboxyl end group. The percent total ion current data for species 1-1Li fragmentation are given in the sixth column of Table 4. The species observed for CID fragmentation are, with one exception, the same species as those observed for the 1-1 oligomer, allowing for differences in mass due to Li exchange. In fact, many of the relative intensities are quite comparable. The major significant difference occurs for species DOH and CD(1). These are the two main species produced by charge-remote fragmentation as shown in Scheme 1A. The largest %TIC for species 1-1 is for DOH at 29.6%, with CD(1) coming in second at 18.0 %TIC. In the case of species 1-1Li, the largest %TIC is for CD(1)Li at 24.3% with DOH showing only 11.0% TIC. It is difficult to postulate a probable cause for this difference. The peak at 122 Da observed for OOLi(1), the Li exchanged species of OOH(1), is the third most intense peak in the spectrum of 1-1Li at 15.9%TIC. Again, there seems to be no apparent reason for this difference beyond the known effect of Li cationization to produce more intense low mass species in CID. Of particular interest is the peak at 363 Da (HOOLI) shown in Scheme 1B, reaction B-1; it corresponds to a Li-exchanged species with retention of charge. Li addition may stabilize a normally unstable phenoxy radical.

3.3.3 Precursor Structure 1-2—The next precursor ion of interest is the di-hydroxyl terminated oligomer (Structure 1-2, 837.2 Da, $n = 3$). It is essentially structure 1-1 with an additional 1,4-dihydroxybenzene end group. The CID fragmentation spectrum of the $n = 3$ oligomer is shown in Figure 4; the percent total ion current data are summarized in the third column of Table 4. Inspection of Fig. 4 reveals a series of low mass fragment ions and two major species above mass 200 Da, due to DOH and BOH*. This is consistent with Scheme 1. Scheme 1A indicates that charge-remote fragmentation will produce the same fragments (DOH) in both Reactions A-1 and A-2 because of the identical end groups. Similarly, Scheme 1B shows production of species BOH* by both Reactions B-1 and B-2 by charge-site fragmentation. In addition, species DOH* is produced by an analog of Reaction B-3 in Scheme 1B. These five species account for nearly 60% of the %TIC.

Characteristic of the CID of lithiated species, five small fragment ions account for 38.2%TIC: DB*, OOH(1), BB(1)*, and OO. The remaining species (4.3% TIC), at 665 and 905 Da, are labeled “XXX*”, because it is difficult to suggest a reasonable structure. XXX*

results in a peak at 665 Da for the 837 Da oligomer, and one at 905 Da for the 1077 Da oligomer at a mass of M-172 in each case. Loss can be accounted for by a combination of 1 C₆H₄, 1 hydroxyl, 2 carbonyls, 1 oxygen and 1Li. A structure fitting this combination would be HOOC-Ph-COOLi. This would require that the 665 Da peak consist of 6 C₆H₄ groups, 4 carbonyl groups, 6 oxygens and 1 hydrogen. A plausible structure is shown for XXX* in Table 3. The difficulty with this is that forming both the 172 loss and 665 Da structures would require removal of a segment of the polymer chain and subsequently rejoining the chain at the fracture point. Another possible reaction sequence would be to have the 665 Da structure formed by loss of 35 Da (Li+CO) from the DOH fragment at 700.2 Da. However, this suffers from the same problem as above; we have been unable to find precedent for either set of reactions.

3.3.4 DHB-T Precursor Structure 1-3—Figure 5A shows a MALDI-TOF/TOF CID spectrum for the dicarboxyl-capped structure of DHB-T (1-3, 653.1 Da, $n = 2$). The percent total ion current data are summarized in the fourth column of Table 4. Using C(O)-O bond cleavage as the focal point, the species specific fragmentation mechanism for a dicarboxyl-capped DHB-T structure can be understood using Scheme 1. Three major species are observed. Species CD(1) is produced by both Reactions A-1 and A-1 in Scheme 1A because the oligomer has identical end groups. Similarly, CB* is produced by Reactions B-1 and B-2 in Scheme 1B; CD(2)* is produced by Reaction B-3 in Scheme 1B. Together, these account for 72.1%TIC.

In addition, two small fragments are produced, OO and DB*, typical of Li cationized oligomers, the latter in significant quantity as was the case for Species 1-1. Formation of CBLi accompanies CB* production, again as for Species 1-1. The OOH(2) fragment at 504 Da (8.9% TIC) is an oddity; it corresponds to a mass loss of M-149 from the 1-3 oligomer at 653 Da. Loss of mass 149 could result from loss of the polymer end group, as shown in Scheme 2A. Fragmentation of the C(O)-O bond is reasonable based on bond energies, but terminal oxygen radicals generally have not been stable species in polymer MS/MS. It could be that during fragmentation the Li is transferred to the phenoxy oxygen with charge transfer to the organic moiety, as was suggested for structure XXX*. The 504 Da structure is shown as OOH(2) in Table 3.

3.3.5 DHB-T Precursor Structure 1-3Li—Figure 5B shows the MALDI-TOF/TOF CID spectrum for the lithium cationized, lithium exchanged di-carboxyl terminated oligomer of DBH-T (Structure 1-3Li, 659.1 Da, $n = 2$). Exchange has occurred between Li and H at a carboxyl end group. The species observed for CID fragmentation of the Li-exchanged oligomer are mostly the same as those observed for the 1-3 oligomer, allowing for differences in mass due to Li exchange. The lithiated three major fragment ions described in Scheme 1, CD(1), CD(2)*, and CB*, account for 68% TIC in the right-hand column of Table 4. The other major fragments are DB* and DB along with the minor fragment OO. It is interesting to note that, although the sum of the major fragmentation processes is similar for the 1-3 and 1-3Li oligomers, the major process for oligomer 1-3 is that of Scheme 1A (charge-remote fragmentation) but for the 1-3Li oligomer it is Scheme 1B (charge-site fragmentation). In addition, the DB species fragmentation is increased for the 1-3Li

oligomer, consistent with increased charge-site fragmentation in the lithiated oligomer. One unique fragment ion is detected for the 1-3Li oligomer BB(2) at 515.0 Da, 6.5% TIC; a possible structure is shown in Table 3. A double carbonyl terminated structure is consistent with the mass observed, as shown in Scheme 2B. Although this structure should be stable, it is difficult to see how it could be produced from the 659 Da oligomer, the C(O)-OH bond energy is the strongest in the molecule (see Fig. 1) and the adjacent C(O)-phenyl bond is weaker. The only possibility would be for a Li-induced rearrangement at the terminal carboxyl group to cause loss of LiO-Ph-COOH with charge transfer to the organic moiety.

3.3.6 DHB-T Precursor Structure 1-1N—Figure 6 shows the MALDI-TOF/TOF CID spectrum for the hydroxyl-diethylamine terminated oligomer of DBH-T (Structure 1-1N, 800.2 Da, $n = 3$). This oligomer is probably produced by reaction of oligomer 1-1 with the diethylamine added to take up HCl produced during the synthesis reaction. The percent total ion values are given in the fifth column Table 4. Most of the fragments listed in Table 4 would be predicted by the mechanisms of Scheme 1, ND(1) and DOH are formed by charge-remote fragmentation as per Scheme 1A. BOH* and NB* are the products predicted by Scheme 1B for charge-site fragmentation. The major fragments represent 62.5% TIC. Fragment ND(2) (Reaction B-3) is weak as it is for oligomer 1-1. Species DB, DB* and BB* are small fragments common to the other oligomer MS/MS spectra.

The two unique fragments observed for oligomer 1-1N are ND(3) and QQQ. Fragment ND(3) formally corresponds to replacement of an ethyl group on the amide nitrogen with a hydrogen. Most likely this occurs by a 1,5 H-transfer [13] as shown in Scheme 3. A terminal hydrogen of the ethyl group is ideally positioned for reaction with the amide carbonyl. Hydrogen abstraction causes loss of ethylene, yielding a tautomer of the secondary amide, ND(3). The C(O)-N bond (vi in Fig. 1) is weaker than the other bonds in the molecule, except for the C(O)-O bond (iii in Fig. 1). One might anticipate, based on bond energies, seeing a peak at M-100 Da caused by fracture of the C(O)-N bond and subsequent loss of CO as is observed for charge-remote fragmentation in Scheme 1A. However, the proximity of the carbonyl group and an aliphatic hydrogen (Scheme 3) allows 1,5 H-transfer to trump direct chain fracture, leading to loss of ethylene.

Species QQQ is another matter. As can be seen from Fig. 6, it occurs as a clump of peaks, separated by 2 Da, the center of which is at 648 Da, corresponding to M-152. Attempts at trying to find a reasonable structure for either the 648 Da peak or for the 152 Da loss were not successful. The only reasonable possibility seemed to be that it is formed by a secondary loss of 15 Da from the ND(1) fragment at 663 Da. The possibility would be for formation of a four-membered ring from the two ethyl groups with varying loss of hydrogen, thus accounting for the multiple peaks observed.

3.4 Relationship to Other Polymers

The study of DHB-T polyesters was begun for two reasons. First, no studies have been reported on the mass spectrometry of totally aromatic polyesters, presumably because of their poor solubility in common organic solvents. The E-G sample preparation method yielded spectra of low molecular weight oligomers, up to ca. 2500 Da. This allowed us to

obtain CID spectra to elucidate the decomposition pathways of totally aromatic polyesters. Second, we were interested in seeing how fragmentation reactions occur in polyesters that do not have easily extractable hydrogen atoms. This makes it interesting to compare DHB-T with other polymers, such as aliphatic polyesters and aramids.

Comparison with aliphatic polyesters will be based on our recent study of poly(butylene adipate)(PBA) [5]. The weakest link in PBA polymers is the C(O)-O bond, yet fracture of this bond does not constitute a major pathway in their low-energy fragmentation patterns. Hydrogen transfers dominate fragmentation: 1) 1,5 H-transfer of a diol β -methylene hydrogen atom to a carbonyl; 2) 1,3 H-transfer of an acid α -hydrogen atom to the diol oxygen; and 3) remote cross-chain hydrogen abstraction by a carbonyl. Of these, 1,5-H transfer is dominant. Similarly, the CID fragmentation of polyester-based polyurethanes is dominated by 1,5-H and 1,3-H transfer reactions [11].

Aramids are similar to aromatic polyesters because, typically, they are insoluble and do not contain aliphatic hydrogens, although they do have N-H groups. In aramids the weakest bond is C(O)-NH. Fracture of this bond, and subsequent loss of CO to form a stable phenyl radical, accounts for about 50% TIC in the CID of poly(ρ -phenylenediamine terephthalamide) (PPD-T) [1], paralleling the major process in DHB-T. Two reactions compete with C(O)-NH bond fracture in PPD-T, both of which, of course, involve H-transfer. In one case, long-range H-transfer from an N-H group to the phenyl radical ring produces a different phenyl radical accounting for about 25% TIC. Cross-chain H-transfer causes fragmentation of the Ph-C(O) bond to produce a terminal-NCO group accounting for about 12% TIC.

All of the above stresses the dominance of H-transfer reactions in CID of polymers when possible. DHB-T provides an additional example noting that the diethylamine terminated oligomer is the only DHB-T species that shows an H-transfer reaction.

4. Conclusions

MALDI spectra of aromatic polyesters were obtained using the evaporation grinding sample preparation method for Na- and Li-cationization. Three major species were observed, based on measurement of percent total ion current: oligomers having hydroxyl-carboxyl, carboxyl-carboxyl, and hydroxyl-hydroxyl end groups. Minor species having end-group modification were decarboxylated phenyl and diethylamino groups, both likely side products from synthesis, along with 3-aminoquinoline adducts from the MALDI process. Lithium cationized spectra typically showed significantly greater low-mass fragmentation than their sodium counterparts. Collision-induced dissociation spectra were obtained for Li-cationized oligomers (better S/N ratios) allowing clear definition of polymer end groups. Two major fragmentation mechanisms were observed, charge-remote and charge-site fragmentation, independent of specific end groups. The major charge-remote fragmentation process was initial scission of the carbonyl-oxygen ester bond with subsequent loss of CO to form a stable phenyl radical terminal group. Charge-site fragmentation involved Li cleavage of the ester group with formal charge transfer to the organic moiety, yielding either a carbonyl or

phenyl terminated radical ion having intrinsic charge. When end groups contained aliphatic hydrogens, 1,5-H transfer occurred.

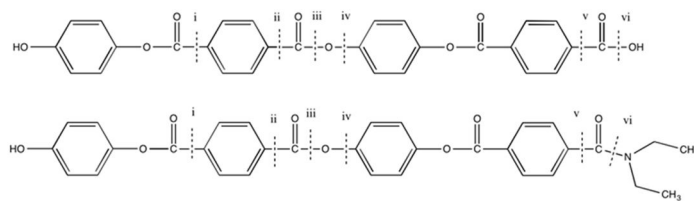
Acknowledgments

We wish to thank Profs. Ned Porter and Terry Lybrand for valuable discussions. Financial support for S. S. and J. A. M. was provided by the National Institutes of Health (5UH2RT000491-2). Partial support for A. P. G. was provided by Chevron Phillips Chemical Company LLP.

References

1. Gies AP, Ellison ST, Stow SM, Hercules DM. *Anal Chim Acta*. 2014; 808:124–1432. [PubMed: 24370099]
2. Wesdemiotis C, Solak N, Polce MJ, Dabney DE, Chaicharoen K, Katzenmeyer BC. *Mass Spectrom Rev*. 2011; 30:523–559. [PubMed: 20623599]
3. Polce, MJ.; Wesdemiotis, C. MALDI mass spectrometry for synthetic polymer analysis. Li, L., editor. Hoboken, NJ: John Wiley & Sons, Inc; 2010. p. 85-127.
4. Rizzarelli P, Puglisi C, Montaudo G. *Rapid Commun Mass Spectrom*. 2006; 20:1683–1694. [PubMed: 16645991]
5. Gies AP, Ellison ST, Chakraborty AK, Kwiecien NW, Hercules DM. *RSC Advances*. 2012; 2:4135–4151.
6. Pretorius NO, Rode K, Simpson JM, Pasch H. *Anal Chim Acta*. 2014; 808:94–103. [PubMed: 24370096]
7. Pretorius NO, Willemese CM, de Villiers A, Pasch H. *J Chromatog A*. 2014; 1330:74–81. [PubMed: 24472839]
8. Gies AP, Hercules DM, Ellison ST, Nonidez WK. *Macromolecules*. 2006; 39:941–947.
9. Gaymans, RJ. *Synthetic Methods in Step-Growth Polymers*. In: Rodgers, ME.; Long, TE., editors. *Synthetic methods in step-growth polymers*. Hoboken, NJ: John Wiley & Sons, Inc; 2003.
10. Frisch, MJ.; Trucks, GW.; Schlegel, HB.; Scuseria, GE.; Robb, MA.; Cheeseman, JR.; Scalmani, G.; Barone, V.; Mennucci, B.; Petersson, GA.; Nakatsuji, H.; Caricato, M.; Li, X.; Hratchian, HP.; Izmaylov, AF.; Bloino, J.; Zheng, G.; Sonnenberg, JL.; Hada, M.; Ehara, M.; Toyota, K.; Fukuda, R.; Hasegawa, J.; Ishida, M.; Nakajima, T.; Honda, Y.; Kitao, O.; Nakai, H.; Vreven, T.; Montgomery, JA., Jr; Peralta, JE.; Ogliaro, F.; Bearpark, M.; Heyd, JJ.; Brothers, E.; Kudin, KN.; Staroverov, VN.; Kobayashi, R.; Normand, J.; Raghavachari, K.; Rendell, A.; Burant, JC.; Iyengar, SS.; Tomasi, J.; Cossi, M.; Rega, N.; Millam, JM.; Klene, M.; Knox, JE.; Cross, JB.; Bakken, V.; Adamo, C.; Jaramillo, J.; Gomperts, R.; Stratmann, RE.; Yazyev, O.; Austin, AJ.; Cammi, R.; Pomelli, C.; Ochterski, JW.; Martin, RL.; Morokuma, K.; Zakrzewski, VG.; Voth, GA.; Salvador, P.; Dannenberg, JJ.; Dapprich, S.; Daniels, AD.; Farkas, O.; Foresman, JB.; Ortiz, JV.; Cioslowski, J.; Fox, DJ. *Gaussian 09, Revision A.02*. Wallingford CT: Gaussian, Inc; 2009.
11. Gies AP, Hercules DM. *Anal Chim Acta*. 2014; 808:199–219. [PubMed: 24370105]
12. Wampler, TP. *Applied Pyrolysis Handbook*. 2. Boca Raton, FL: CRC Press; 2007.
13. Moldoveanu, SC. *Analytical Pyrolysis of Synthetic Organic Polymers*. New York: Elsevier; 2005.

- First MALDI collision-induced dissociation study of wholly aromatic polyesters
- Effect of polymer end groups and bond energies on collision-induced mass spectra
- Effect of end groups on polymer fragmentation mechanisms
- Fragmentation mechanisms compared to those for aliphatic polyesters and aramids
- Both charge-site and charge-remote fragmentation reactions observed



Bond	Acid-ol Terminated		Amide-ol Terminated	
	Energy (Doublet) kcal./mol	Energy (Triplet) kcal./mol	Energy (Doublet) kcal./mol	Energy (Triplet) kcal./mol
i	95.45	95.38	95.29	95.28
ii	106.21	106.19	106.58	105.37
iii	64.77	64.75	64.79	64.75
iv	96.94	96.85	97.18	97.13
v	107.53	107.46	92.02	91.94
vi	112.22	112.21	83.24	83.23

Figure 1. Model compounds and bond energy calculations for acid-ol and amide-ol terminated aromatic polyesters. See text for details.

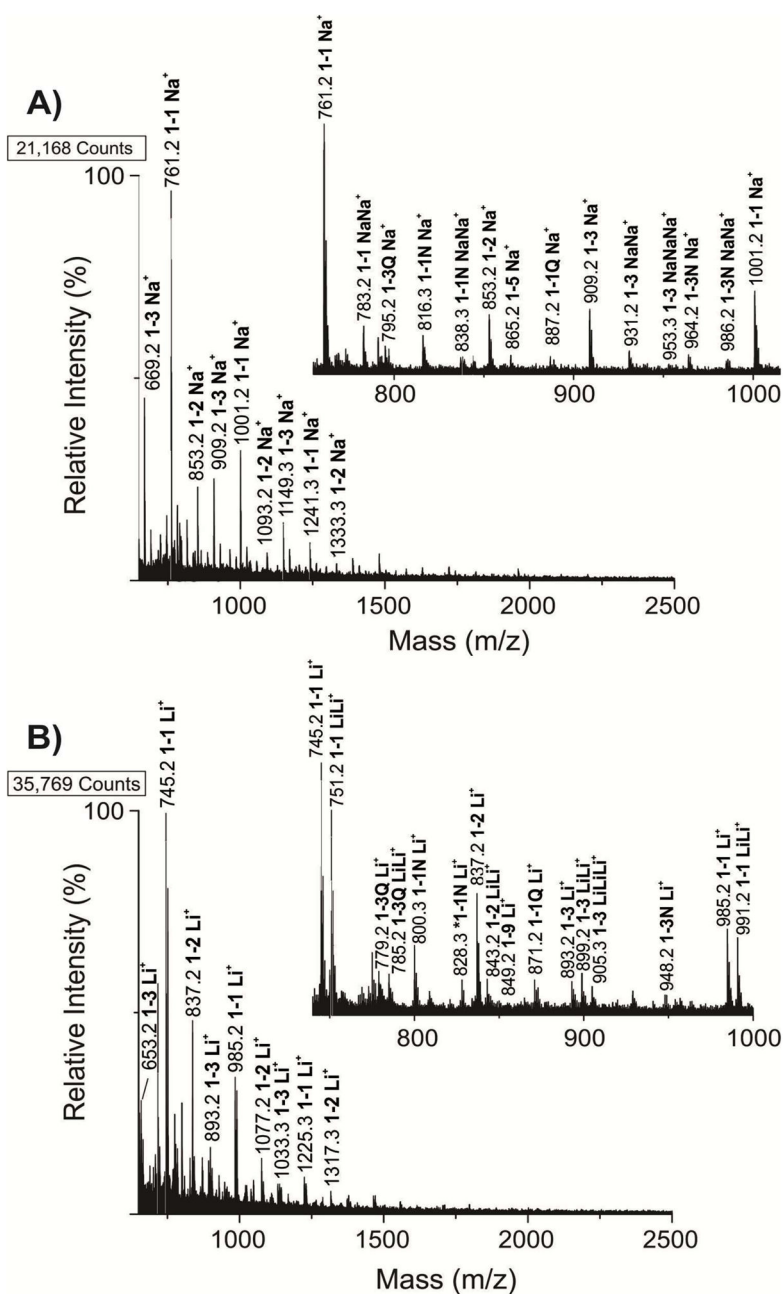


Figure 2. MALDI-TOF mass spectra of DHB-T aromatic polyesters for A) Sodium cationized spectrum and B) Lithium cationized spectrum. Insets show spectral detail in the approximate range of 750 – 1000 Da. Samples prepared by the E-G method in 3AQ and cationized with NaTFA and LiTFA.

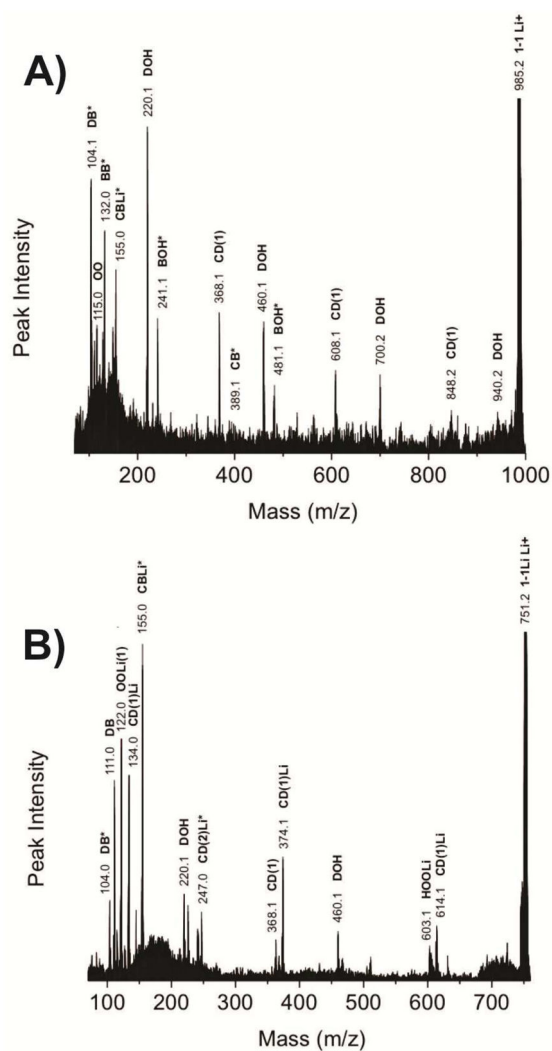


Figure 3. Low effective kinetic energy (collision gas pressure: 5×10^{-6} Torr) ABI 4700 MALDI-TOF/TOF CID mass spectra Samples prepared by the E-G method in 3AQ and cationized with LiTFA. A) Hydroxyl-carboxyl capped DHB-T oligomer (species 1-1Li⁺) – 985.2 Da precursor ion. B) Hydroxyl-carboxyl capped DHB-T oligomer, end-group modified by Li exchange (species 1-1LiLi⁺) – 751.2 Da precursor ion.

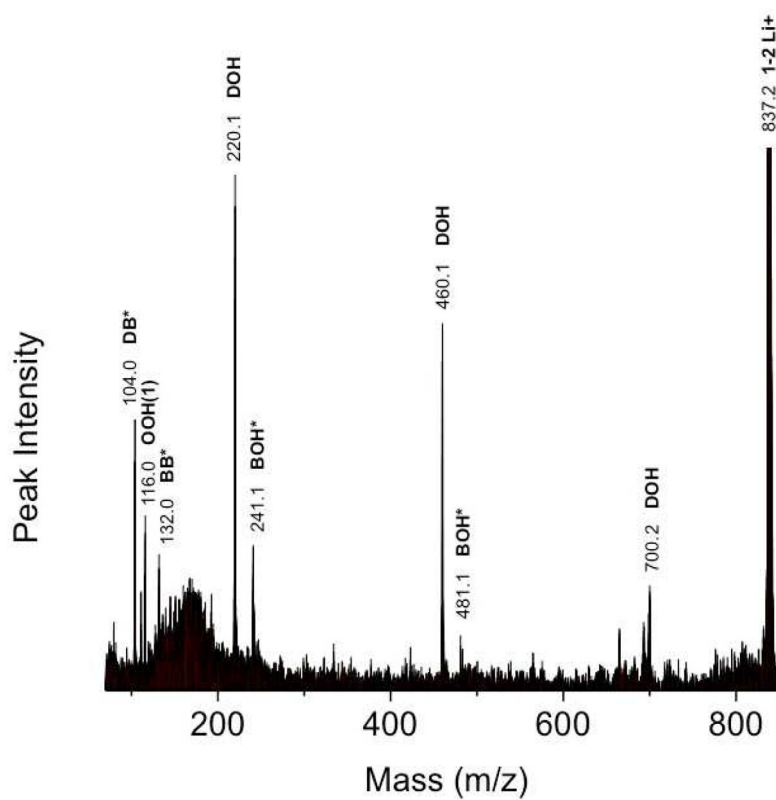


Figure 4. Low effective kinetic energy (collision gas pressure: 5×10^{-6} Torr) ABI 4700 MALDI-TOF/TOF CID mass spectrum of a hydroxyl-hydroxyl capped DHB-T oligomer (species 1-2Li⁺) – 837.2 Da precursor ion. Samples prepared by the EG method in 3AQ and cationized with LiTFA.

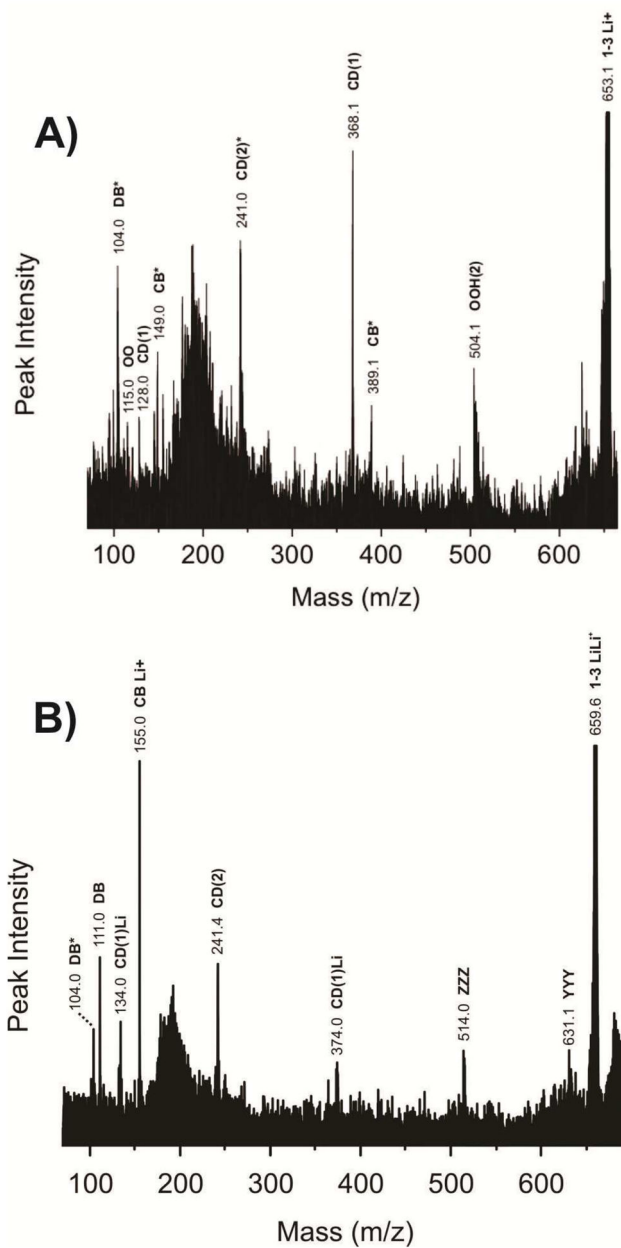


Figure 5. Low effective kinetic energy (collision gas pressure: 5×10^{-6} Torr) ABI 4700 MALDI-TOF/TOF CID mass spectra. Samples prepared by the E-G method in 3AQ and cationized with LiTFA. A) Carboxyl-carboxyl capped DHB-T oligomer (species 1-3Li⁺) – 653.1 Da precursor ion. B) Carboxyl-carboxyl capped DHB-T oligomer, end-group modified by Li exchange (species 1-3LiLi⁺) – 659.1 Da precursor ion.

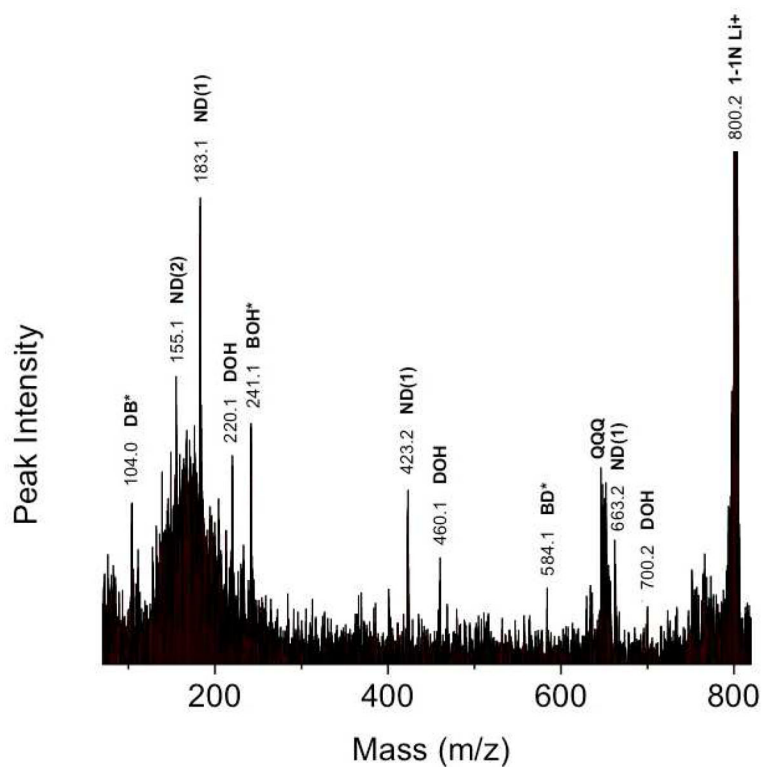
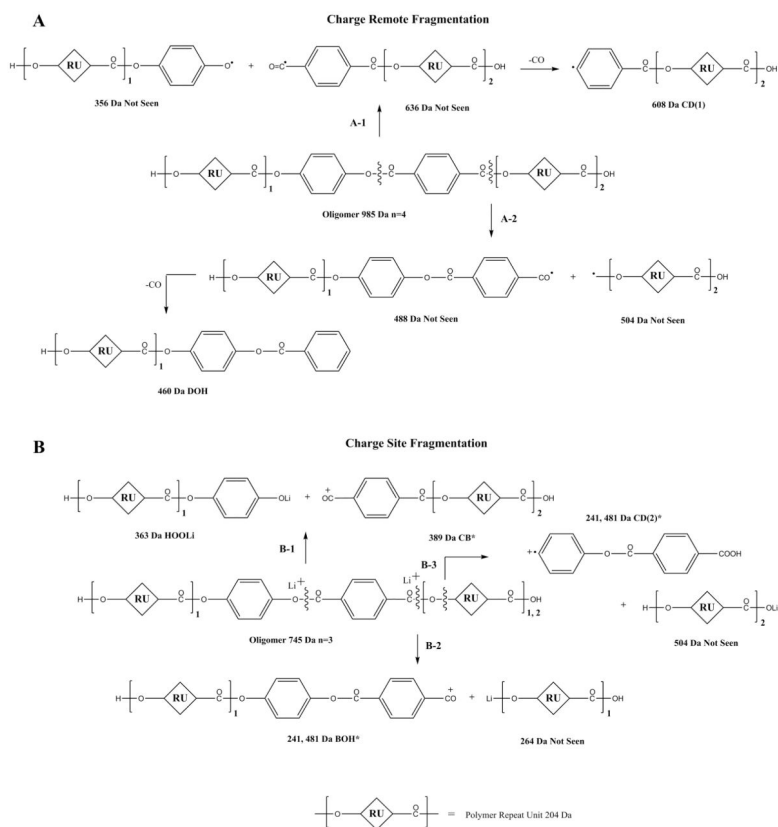
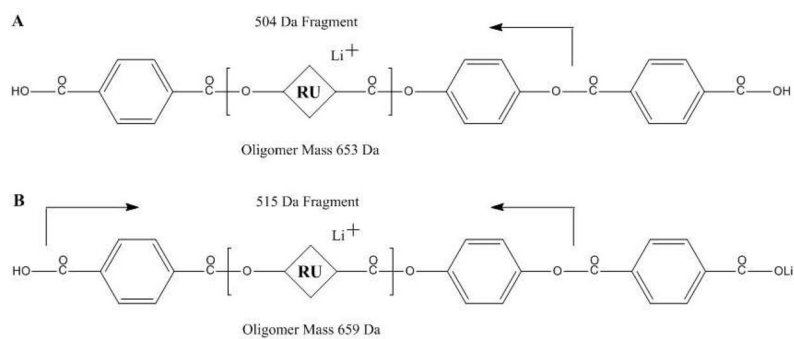


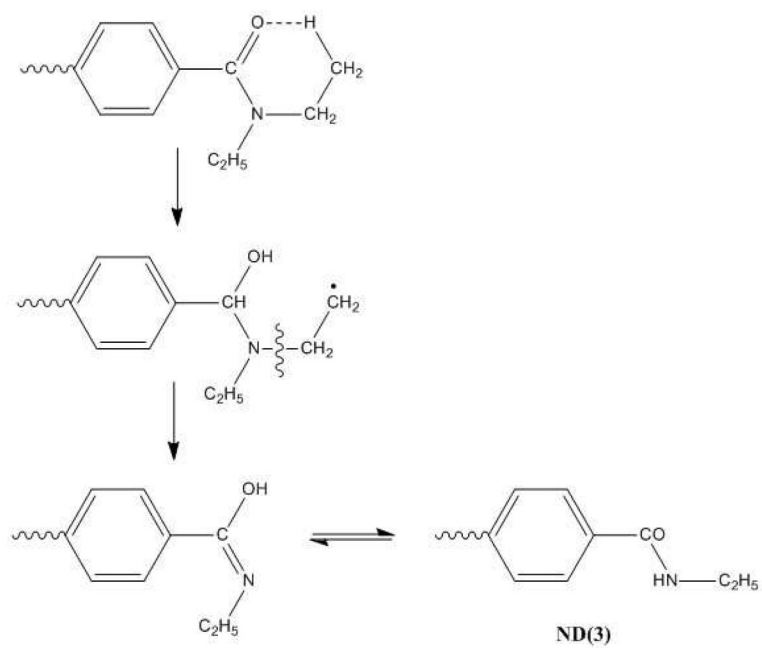
Figure 6. Low effective kinetic energy (collision gas pressure: 5×10^{-6} Torr) ABI 4700 MALDI-TOF/TOF CID mass spectrum of a hydroxyl-carboxyl capped DBH-T oligomer, end-group modified with diethylamine (species 1-1N Li^+) – 800.2 Da precursor ion. Samples prepared by the E-G method in 3AQ and cationized with LiTFA.

**Scheme 1.**

Major fragmentation mechanisms for the hydroxyl-carboxyl terminated aromatic polyester tetramer (985.2 Da) for A) Charge-remote fragmentation and B) Charge-site fragmentation.

**Scheme 2.**

Fragmentation mechanisms for carboxyl-carboxyl terminated aromatic polyester species for A) 1-3 Li⁺ dimer (653.1 Da) and B) 1-3 LiLi⁺ dimer (659.2 Da).

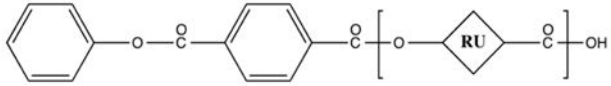
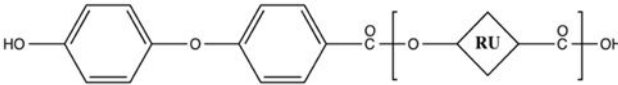
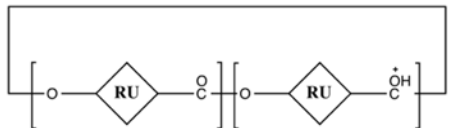
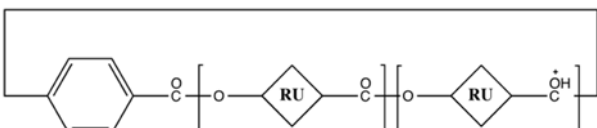


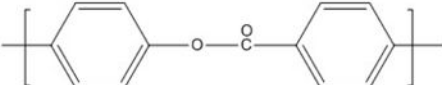

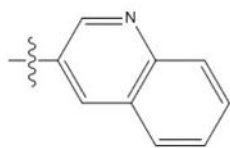


Scheme 3.
1,5-Hydrogen transfer fragmentation mechanism for the hydroxyl-amide terminated polyester (1-1NLi⁺).

Table 1

Structural assignments for aromatic polyester parent-ion species. Data are for Na- and Li-cationized MALDI spectra. Masses are given for mid-range ions. Species in brackets <> are for metal ion-exchanged species. Q - Matrix adduct. N - diethylamino end group. n - Number of repeat units. M - Metal ion (Na or Li).

Aromatic Polyester Parent Ion Species			
Species	Structure	Mass Na Adduct	Mass Li Adduct
1-1 <1-1M>		521.1 (n=2) 761.2 (n=3) <543.1 (n=2)>	505.1 (n=2) 745.2 (n=3) <751.2 (n=3)>
1-1N <1-1NM>		576.2 (n=2) 816.3 (n=3) <838.3 (n=3)>	560.2 (n=2) 800.2 (n=3) Not Observed
1-1Q		887.4 (n=3)	871.3 (n=3)
1-2		613.2 (n=2) 853.3 (n=3)	597.1 (n=2) 837.2 (n=3)
1-3 <1-3M> <1-3MM>		669.2 (n=2) 909.3 (n=3) <691.2 (n=2)> Not Observed	653.1 (n=2) 893.2 (n=3) <659.2 (n=2)> <665.3 (n=2)>
1-3N <1-3NM>		724.3 (n=2) 964.4 (n=3) <986.3 (n=3)>	708.2 (n=2) 948.2 (n=2) Not Observed
1-3Q		795.3 (n=2)	779.4 (n=2)
1-4		717.2 (n=2) 957.3 (n=3)	701.2 (n=2) 941.4 (n=3)
1-5 <1-5M>		625.3 (n=2) <647.2 (n=2)>	609.2 (n=2) Not Observed
1-6 <1-6M>		597.2 (n=2) 837.3 (n=3) <619.3 (n=2)>	581.2 (n=2) Not Observed

Aromatic Polyester Parent Ion Species			
Species	Structure	Mass Na Adduct	Mass Li Adduct
1-7		745.3 (n=2) 985.4 (n=3)	729.3 (n=2) 969.3 (n=3)
1-8 <1-8M>		Not Observed	717.3 (n=2) 957.3 (n=3) <723.3 (n=2)> <963.3 (n=3)>
Cyclic(1)		481.2 (n=2)	Not Observed
Cyclic(2)		585.3 (n=2)	Not Observed
Key	<p>Polymer Repeat Unit = </p> <p> = </p> <p> = </p>	<p>Mass 240 Da 196 Da 128 Da</p>	


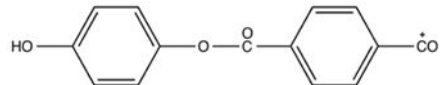

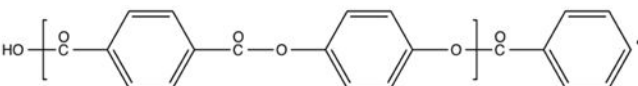
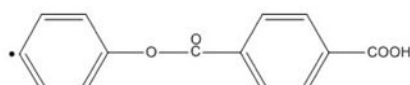
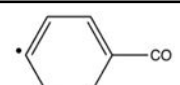
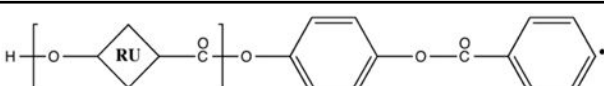
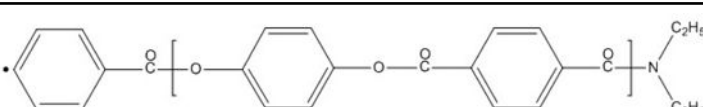
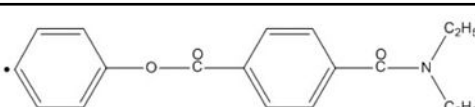
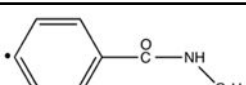
Percent total ion current (% TIC) for DHB-T parent-ion species for A) (left side) All species from Table 1 and B) (right side) Combined species for parent oligomers (See text).

Table 2

Species	2L-MALDI Percent Total Ion Current Species Observed		2R-MALDI Percent Total Ion Current DHB-T Oligomers		
	Cationization (M)		Oligomer	Cationization (M)	
	Na	Li		Na	Li
1-1	15.7	14.1	1-1	30.8	43.8
1-2	11.3	12.8	1-3	26.6	17.9
1-3	8.5	4.3	1-2	11.3	12.8
1-3Q	6.9	1.9	1-5	9.4	4.7
1-1M	6.8	13.2	1-6	8.4	4.2
1-6	6.0	4.2	1-7	4.7	0.7
1-5	5.6	4.7	Cyclic(1)	3.7	Not Observed
1-1N	5.5	7.6	1-4	3.3	1.6
1-7	4.7	0.7	Cyclic(2)	1.7	Not Observed
1-3M	4.6	6.0	1-8	Not Observed	14.2
1-5M	3.8	Not Observed			
Cyclic(1)	3.7	Not Observed			
1-3N	3.4	2.4			
1-4	3.4	1.6			
1-3NM	3.3	Not Observed			
1-6M	2.3	Not Observed			
1-1Q	2.0	8.9			
Cyclic(2)	1.7	Not Observed			
1-1NM	0.7	Not Observed			
1-8	Not Observed	8.9			
1-8M	Not Observed	5.3			
1-3MM	Not Observed	3.3			

Table 3

Aromatic polyester MS/MS fragment-ion species. Masses are given for prominent peaks observed. Species having intrinsic charge are indicated by an asterisk (*); all others are Li cationized.

Aromatic Polyester Fragment Ion Species		
Species	Structure	Masses
BB(1)* BB(2)		132.02 515.01
BOH*		241.01, 481.01
CB* <CBLi*>		149.01, 389.06 <155.02>
CD(1) <CD(1)Li*>		368.04, 608.03 <374.03, 614.03>
CD(2)* <CD(2)Li*>		241.01, 481.01 <247.03>
DB DB*		111.04 104.01
DOH <DOHLi*> DOH*		460.07, 700.09 <466.16, 706.14> 693.11
ND(1)		423.11, 663.33
ND(2)		303.03
ND(3)		155.02



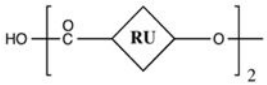
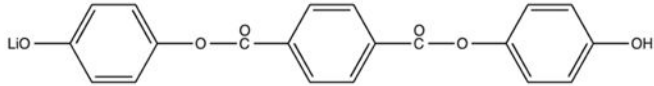
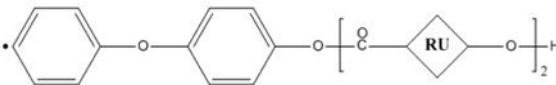
Aromatic Polyester Fragment Ion Species		
Species	Structure	Masses
OO		115.04
OOH(1) <OOLi(1)>		116.03 <122.02>
OOH(2)		504.01
<HOOLi>		<363.02>
XXX*		665.17, 905.36

Table 4

MS/MS Percent total ion current for all DHB-T oligomers/species. A) For each oligomer/species fragment ions are listed in the column along with their average %TIC values. B) The first column (Scheme 1) identifies the nature of the species. The first five lines (marked A1-B3) are fragments identified in Scheme 1. The sixth line is the sub-total for the %TIC values for A1-B3. C) The next four lines are for small fragments that are common to most species. D) The last two lines are for species characteristic of individual species. See text for discussion.

Scheme 1	Oligomer 1-1		Oligomer 1-2		Oligomer 1-3		Oligomer 1-IN		Species 1-1Li		Species 1-3Li	
	Frag.	%TIC	Frag.	%TIC	Frag.	%TIC	Frag.	%TIC	Frag.	%TIC	Frag.	%TIC
A1	CD(1)	18.0	DOH	38.6	CD(1)	30.4	ND(1)	29.5	CD(1)Li	24.3	CD(1)Li	18.0
A2	DOH	29.6	DOH		CD(1)		DOH	16.5	DOHLi	11.0	CD(1)Li	
B1	CB*	14.0	BOH*	15.1	CB*	22.7	BOH*	10.4	CBLi*	19.0	CB*Li	37.1
B2	BOH*	8.2	BOH*		CB*		NB*	6.1		<1	CB*Li	
B3	CD(2)*	<1	DOH*	4.1	CD(2)*	19.3	ND(2)	<1	CD(2)Li*	6.3	CD(2)Li	13.0
Subtotal	---	69.8	---	57.8	---	72.4	---	62.5	---	60.6	---	68.1
Small Fragments	DB*	12.5	DB*	18.4	DB*	13.8	DB*	15.5	DB*	16.1	DB*	22.1
	BB(1)*	7.8	BB(1)*	8.1			BB(1)*	5.0	BB(1)*	3.7		
	OO	5.0	OO	2.6	OO	4.9			OO	2.0	OO	3.3
	OOH(1)	5.0	OOH(1)	9.0					OOLi(1)	15.8		
Unusual Fragments			XXX*	4.3	OOH(2)	8.9	ND(3)	8.6	HOOLi	2.0	BB(2)	6.5
							QQQ	8.4				